

GGG: state of the art and perspectives

Anna M. Nobili and Raffaello Pegna

Prepared for INFN CSNII - Perugia (28 September 2011)

Contents

1	GGG sensitivity to EP violation in the field of the Sun as compared to rotating torsion balances and other ground tests	2
2	GG in space: target signal, thermal noise and evidence of no signal attenuation by rotation above resonance	7
3	GGG sensitivity as compared to target in space	9
4	Assessment of low frequency noise sources	11
4.1	Read-out electronics noise	11
4.2	Tilt and horizontal acceleration noise	12
4.3	Thermal stability	15
5	Attenuation of ball bearings noise and expected improvements	16
6	GGG design with air bearings and optical read-out	18

1 GGG sensitivity to EP violation in the field of the Sun as compared to rotating torsion balances and other ground tests

GGG can test the EP in the field of the Sun by comparing the gravitational attraction from the Sun ($a_{\odot} \simeq 6 \cdot 10^{-3} \text{ m/s}^2$) with the inertial centrifugal acceleration due to the annual revolution of the Earth around the Sun for test masses of different composition. In GGG the test cylinders are both made of the same material (*Al*), so it is used to assess the sensitivity of the apparatus to this test. Because of the diurnal rotation of the Earth the effect is expected at this frequency in the non rotating horizontal plane of the lab; GGG spins (test cylinder and read-out together) in order to up-convert the signal to its spin frequency. After demodulation, the relative displacements of the test cylinders (which should be zero) are reported in the horizontal plane of the lab where the 24 hr effect gives the relevant sensitivity.

The best EP test in the field of the Sun has been achieved by a rotating torsion balance[1] and it rules out a violation to $\eta_{RTB_{\odot}} \simeq 10^{-12}$. Another rotating torsion balance from the same group has achieved $\eta_{RTB_{\oplus}} \simeq 10^{-13}$ but in the field of the Earth[2].

At the diurnal frequency of the Sun $\nu_{\odot} = 1.16 \cdot 10^{-5} \text{ Hz}$ the spectral density of the relative displacements of the GGG test cylinders as reported in Fig. 1 (top plot) is:

$$\frac{\Delta Y_{\nu_{\odot}}}{\sqrt{\text{Hz}}} \simeq 10^{-6} \frac{m}{\sqrt{\text{Hz}}} \quad (1)$$

which means (with a natural coupling frequency $\nu_w = 0.072 \text{ Hz}$) a spectral density of the differential acceleration:

$$\frac{\Delta a_{\nu_{\odot}}}{\sqrt{\text{Hz}}} \simeq 2 \cdot 10^{-7} \frac{\text{m/s}^2}{\sqrt{\text{Hz}}} \quad (2)$$

It has been demonstrated that data can be collected for very long durations (uninterrupted runs for more than 1 month have been performed; interruptions are due only to the need of working on the instrument to improve it). It has also been found that low frequency effects (also at diurnal frequency) decrease as the square root of the integration time t_{int} , being mostly due to tilt/horizontal acceleration noise and to ball bearings noise. Therefore, the differential acceleration sensitivity with an integration time $t_{int} = 30 \text{ d}$ is:

$$\Delta a_{\nu_{\odot}|t_{int}} \simeq 1.2 \cdot 10^{-10} \text{ m/s}^2 \quad (3)$$

yielding (after dividing by the acceleration from the Sun $a_{\odot} \simeq 6 \cdot 10^{-3} \text{ m/s}^2$):

$$\eta_{GGG_{\odot}} \simeq 2 \cdot 10^{-8} \quad (4)$$

which is 20000 times less sensitive than the best ground test in the field of the Sun $\eta_{RTB_{\odot}} \simeq 10^{-12}$ performed with the rotating torsion balance in 1999. Note that –due to their very low torsion frequency– rotating torsion balances are more sensitive than GGG test masses by about a factor 6000 and more sensitive than GG test masses in space by a factor 2; however, they are not suitable for flight.

It is also worth comparing this result with other ground tests of EP performed with apparatus different from torsion balances. There are two of them –both of the mass dropping Galileo type– one with macroscopic test masses and one with cold atoms; in both cases the driving common acceleration of the proof masses is $g \simeq 9.8 \text{ m/s}^2$ (rather than $a_{\odot} \simeq 6 \cdot 10^{-3} \text{ m/s}^2$ as in our case), therefore we shall compare also the sensitivity to differential accelerations. The results of a Galileo-like mass dropping test with macroscopic bodies performed by INFN at CERN were published in 1992 [3]: a single vertical disk made of two halves of different composition was dropped from a height and the rotation which would result from EP violation was recorder by a laser read-out. It achieved $\eta_{INFN-CERN} = \Delta g/g = 7.2 \cdot 10^{-10}$, about 30 times better than (4) with a sensitivity to differential accelerations $\Delta g_{INFN-CERN} \simeq 7 \cdot 10^{-9} \text{ m/s}^2$ about 6 time worse than (3). A Galileo-like mass dropping test with cold atoms, using the isotopes ^{85}Rb and ^{87}Rb , has been performed in 2004 at Max Planck [4]: they have achieved $\eta_{MaxPlanck} \simeq 10^{-7}$, which is 5 times worse than (4) with a sensitivity to differential accelerations $\Delta g_{MaxPlanck} \simeq 9.8 \cdot 10^{-7} \text{ m/s}^2$, which is 8000 times worse than (3).

The result (4) has been obtained from the run reported in Fig. 1 (top plot, see caption), taking the spectral density at $\nu_{\odot} = 1.16 \cdot 10^{-5} \text{ Hz}$. At this frequency a similar value is obtained from raw data with best fit (see bottom plot of the same figure and its caption). Fig. 2 shows for another run in which tilts are controlled actively, how –by fitting to temperature and PZT data– it is possible to significantly reduce low frequency noise. However, Fig. 3 makes it apparent that once the system is weakly suspended and tilts

are reduced by a passive (non rotating) 2-D laminar joint the raw data of the read-out are much better than in the case of active tilt control.

In the case of Fig. 3 (bottom plot) it is possible to analyze the data in lock-in mode with the diurnal motion of the Sun, since we know not only the frequency but also the phase of the signal for which we are assessing the sensitivity of the instrument: the signal should not only have the diurnal frequency, but should also always point to the Sun following its motion during the day, hence only the noise which has these features competes with it. This kind of lock-in detection at diurnal frequency requires runs lasting many days (> 20 or more) and allows the 24 hr effect relevant to EP violation in the field of the Sun to be reduced from the one obtained directly from the raw data. The amount of reduction will depend on the structure of the lab, the local environment around it and the way they respond to the thermal effect off the Sun as it moves around during day and night. It cannot be established a-priori but can only be assessed a-posteriori from long runs real data. Note that this is a classical lock-in detection analysis and we are not selecting any particular day of the run as “more favorable” due to local meteo conditions of that day; although we know that local meteo conditions do affect the system (through their effect on the local environment), they are not reproducible and therefore we cannot rely on them.

Such a lock-in detection analysis is ongoing for a recent long August-September run.

In Sec. 4 we report our assessment of the current level of various low frequency noise sources to pin down the one responsible for the noise level reported in Fig. 1 (bottom plot) and in Secs. 5 and 6 we outline our strategy for improvement as established in collaboration with JPL. The first main step of such improvement is expected for next year.

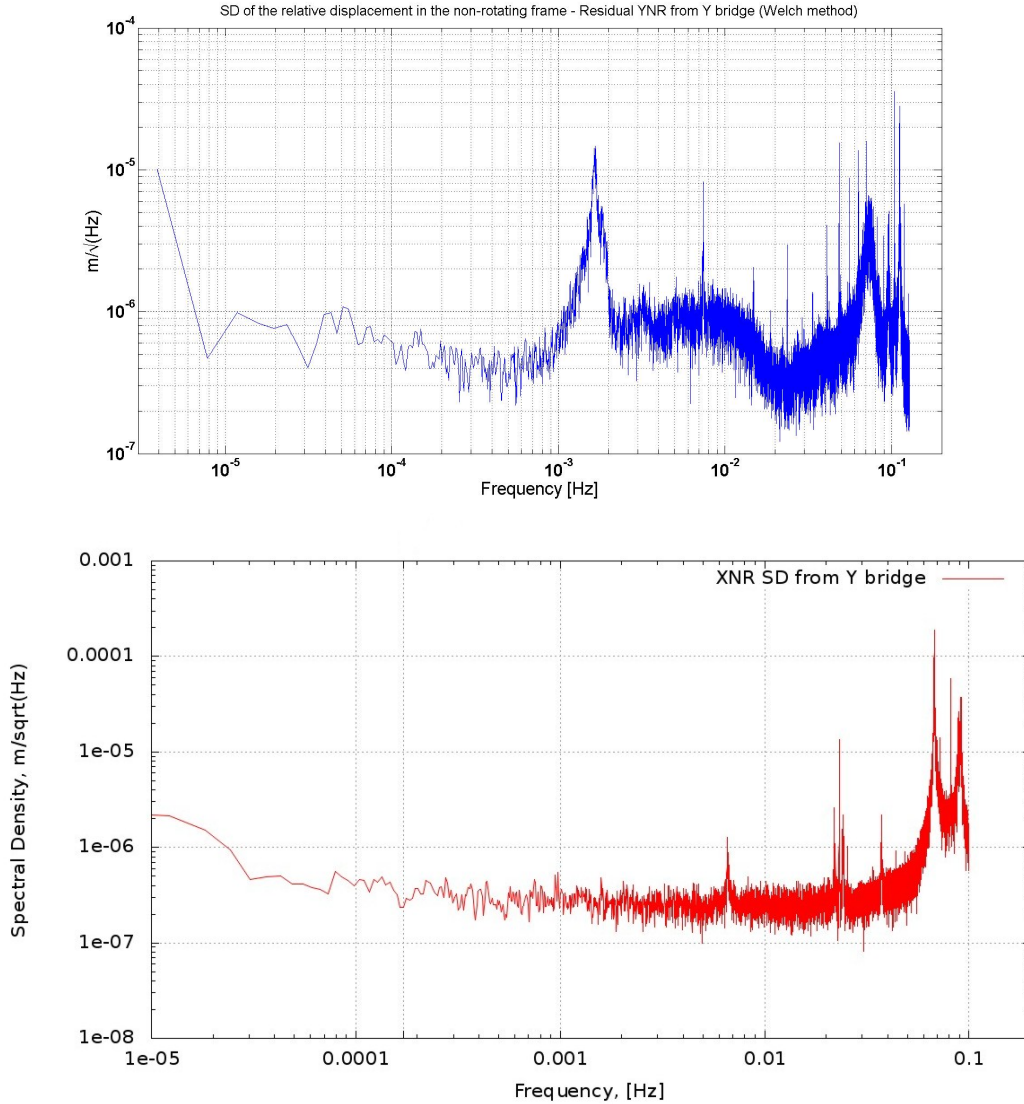


Figure 1: Top plot: Spectral density of the relative displacements of the test cylinders in one direction of the horizontal plane of the lab over 9 days, after demodulation from the rotating system ($\nu_{spin} = 0.257$ Hz). A low frequency tilt control is active (spirit level tiltmeter as sensor and PZTs as actuators) and we record –along with the test masses displacements data– the temperature on the tiltmeter, the temperature on the steel flange housing the ball bearings and the tension applied to the PZTs. This is done because the tiltmeter signal is significantly affected by temperature (especially at low frequencies), and therefore spurious signals are reintroduced into the system by the PZT actuators (especially at the very low frequencies of interest). The result is obtained after fitting to both temperatures and the PZT applied potential (a constant drift is also removed). Correlation with PZT data reduces low frequency noise by about a factor 10, as shown in Fig. 2. The natural coupling frequency of the test masses is $\nu_w = 0.072$ Hz. The large peak above one mHz is due to the water cooling cycle (water cooling was used, along with electric heating, for thermal stabilization). Bottom plot: Spectral density of the relative displacements of the test cylinders in the horizontal plane of the lab ($\nu_{spin} = 0.2$ Hz). The system is passively suspended and no active tilt control is applied (the temperature of the chamber is stabilized by electric heating only). The result is obtained from raw data, no fit or correlation analysis being applied. The natural coupling frequency is 0.09 Hz

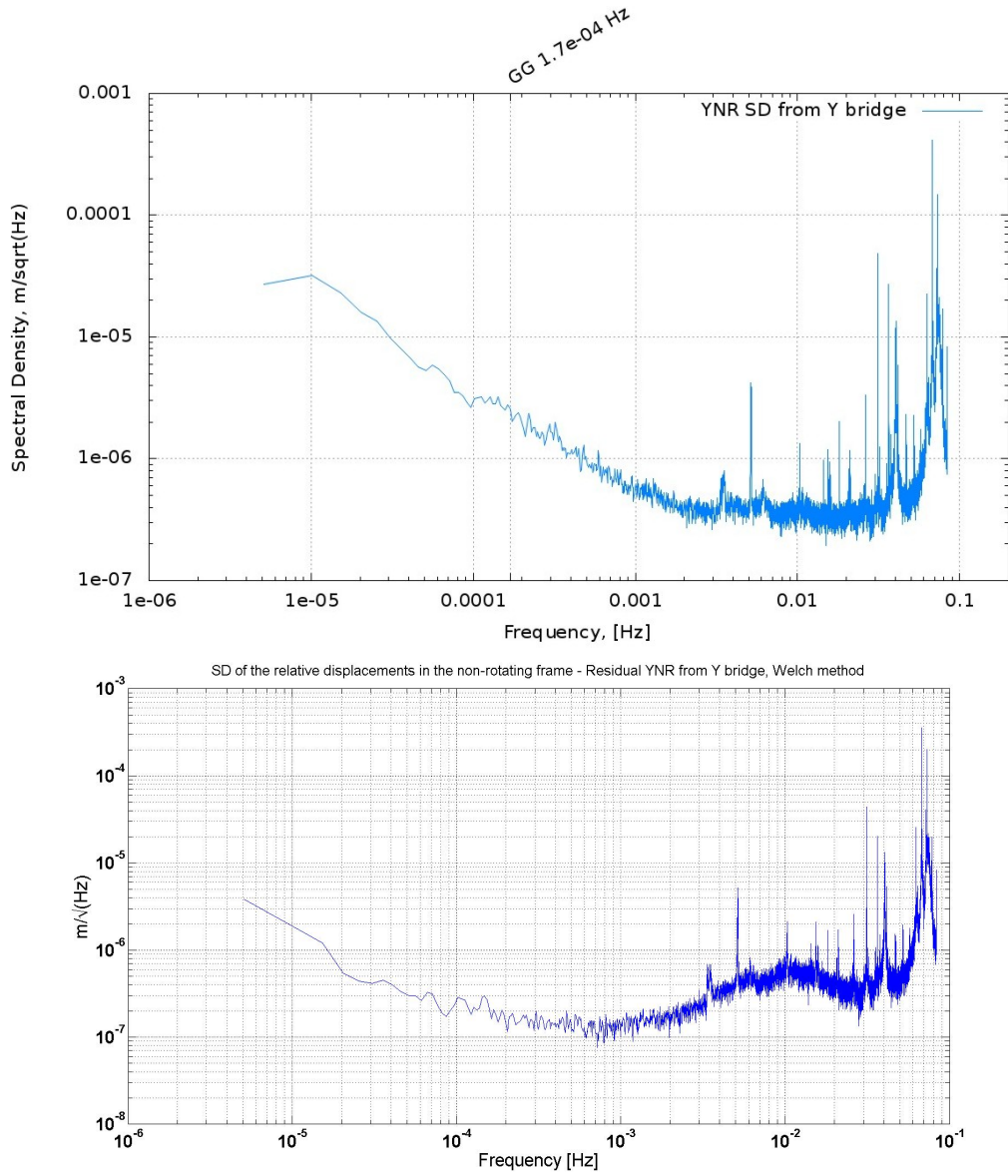


Figure 2: Top plot: Spectral density of the relative displacements of the test cylinders in one direction of the horizontal plane of the lab after demodulation from the rotating system ($\nu_{spin} = 0.166$ Hz, active low frequency tilt control applied with spirit level tiltmeter as sensor and PZTs as actuators, active temperature stabilization by electric heating) as obtained from raw data of the entire run (24.15 d), no fits to temperature or PZT data is applied. Bottom plot: SD for the same data after fitting to temperature and PZT data (13 d data analyzed here). The comparison shows an improvement of a factor 10 at the low frequencies of interest (the diurnal frequency $\nu_{\odot} = 1.16 \cdot 10^{-5}$ Hz and the orbital frequency $\nu_{orb} \simeq 1.7 \cdot 10^{-4}$ Hz at which the signal is expected in the the GG experiment in space)

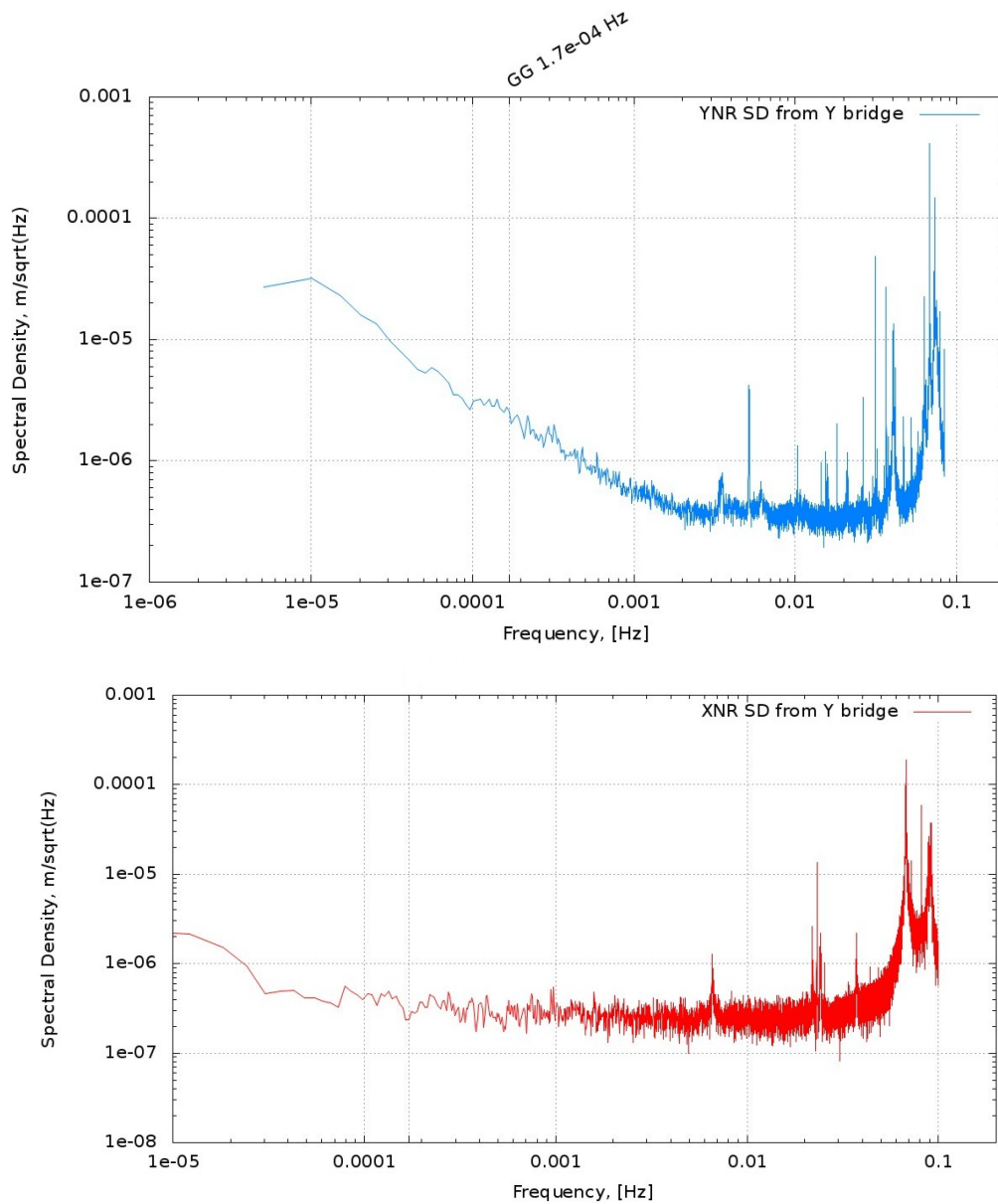


Figure 3: Top plot: Same as the top plot Fig. 2 (active tilt control applied, obtained from raw data, no fit to temperature or PZT data applied) Bottom plot: Same as the bottom plot of Fig. 1 in which –inside the same vacuum chamber– the apparatus is now suspended from a passive 2-D joint (not rotating). These two figures are shown together to make it apparent that the raw data of the new system provide an improvement by a factor 10 at the low frequencies of interest.

2 GG in space: target signal, thermal noise and evidence of no signal attenuation by rotation above resonance

GG aims at testing EP in the field of the Earth to $\eta_{GG} = 10^{-17}$. The signal is at the orbital frequency ν_{orb} of the satellite around the Earth, and is up-converted to the spin frequency ν_{spin} of the satellite. At GG orbiting altitude of about $\simeq 600$ km the target requires to measure a differential acceleration signal Δa_{GG} between proof masses of different composition:

$$\Delta a_{GG} \simeq 8 \cdot 10^{-17} \text{ m/s}^2 \quad (5)$$

acting at frequency $\nu_{orb} \simeq 1/5900\text{s} \simeq 1.7 \cdot 10^{-4}$ Hz in the inertial frame, which is up-converted to $\nu_{spin} = 1$ Hz by the rotation of the GG satellite.

We have demonstrated in [5] that the thermal noise force due to structural damping in the suspensions of the proof masses and competing with the signal up-converted to the spin frequency (after an integration time t_{int}) is:

$$F_{th|t_{int}} \simeq \sqrt{\frac{4K_B T \mu \omega_n^2}{Q \omega_{spin}} \frac{1}{t_{int}}} \quad (6)$$

where: K_B is the Boltzmann constant, T is the equilibrium temperature; $\mu = m/2$ is the reduced mass, i.e. half the mass m of each test body in case of equal masses; ω_n is the frequency of natural oscillations of the proof masses relative to each other; Q is the quality factor of the suspensions expressing their losses at the spin frequency at which they undergo deformations (in GG $m = 10$ kg, $\omega_n = 2\pi/540\text{s}$, $Q = 20000$). According to (6) the high spin frequency of GG compared to similar experiments (by a factor $\simeq 2000$ w.r.t. STEP/GAUGE and Microscope, and by a factor 1200 w.r.t. current rotating torsion balances) allows for a much shorter integration time. We have shown in [6] that in GG –after accounting also for additional thermal noise due to residual gas damping and eddy currents– it is possible to perform in 1 day (corresponding to about 15 orbits, i.e. 15 cycles of the expected signal) a reliable measurement to the required sensitivity. Thanks to this important fact, daily changes in the experiment configuration relative to the Earth (the source mass) allow –over a mission duration of 9 months only– for very powerful null checks capable to discriminate beyond question an EP violation effect (new Physics) from competing classical systematic disturbances. We have demonstrated that this is possible for the known very dangerous effect due to coupling of the monopole of the Earth with the different quadrupole mass moments of the test bodies and for the Earth tidal effects [7].

We have also demonstrated, both theoretically [5] and experimentally (see Fig. 4) that in a 2-D oscillator like GG the signal can be up-converted (by rotating the oscillator) to a frequency much higher than the natural one (in the case of the GG satellite, 1 Hz spin frequency and 1/540s natural frequency) without being attenuated by the ratio $(\omega_n/\omega_{spin})^2$ as it is well known to occur for the 1-D oscillator. In order to appreciate how crucial this fact is, just note that if GG were a 1-D oscillator, the target signal (5) would be attenuated by the huge factor $540^2 = 2.9 \cdot 10^5$, which would clearly amounts to killing it since the effect to be measured, un-attenuated, is about half $pm!$ Thus, up-conversion to high frequency (with the numerous and well known advantages related to it) without killing the signal is possible only with a 2-D oscillator like GG.

We have performed an experimental test with the GGG prototype in order to demonstrate this fact and the results shown here are reported in [8]. In the GGG test, the natural frequency is about 0.1 Hz. A differential force signal at 0.01 Hz in the laboratory frame –i.e. below the resonance– was first applied to the test masses along one direction of the horizontal plane (using the non rotating capacitance plates of whirl control); then the system was set in rotation at the spin frequency of 0.19 Hz, the same differential force being applied. The applied force was therefore up-converted close to the spin frequency; since this is about twice as large as the natural frequency, the force attenuation expected in a 1-D oscillator is by a factor 2.56, which would be well visible in the data, while the measurement clearly shows (see Fig. 4) that no such attenuation is there. This means that in the 2-D GGG oscillator the applied signal has the same amplitude when its frequency is lower than the natural one (non rotating case), and when it is higher than that (rotating case), as it was clearly shown theoretically in [5].

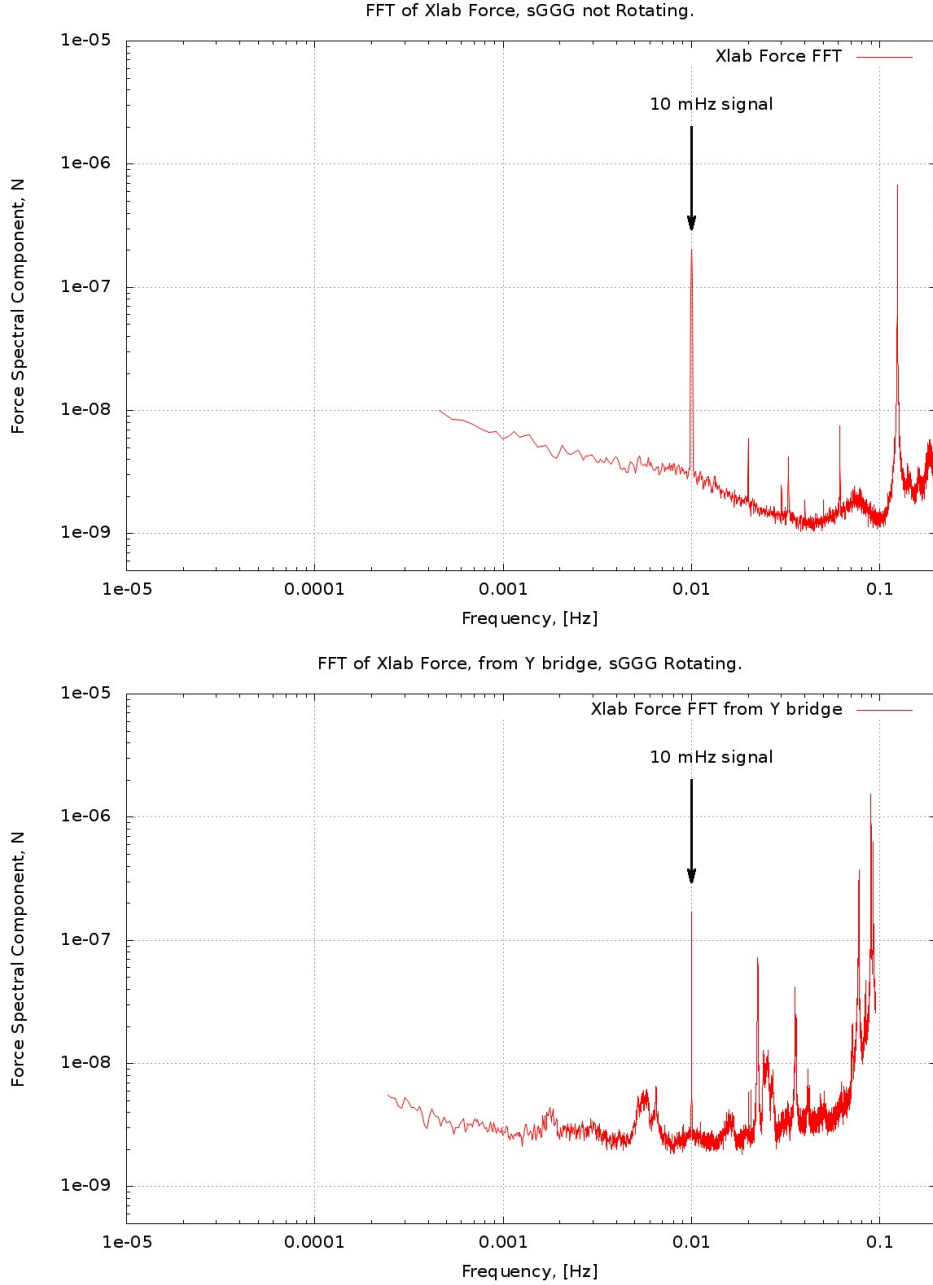


Figure 4: Experimental evidence that in a 2-D oscillator like GGG no signal attenuation occurs above resonance. Top plot: GGG is not rotating and a differential force signal at 0.01 Hz is applied to the test cylinders along the X direction of the horizontal plane of the lab. In this direction the natural frequency of oscillation (resonance) of the test cylinders relative to each other is $\nu_x = 0.124 \text{ Hz}$, thus the force is applied below the resonance. We add that the natural oscillation frequency in the perpendicular direction is $\nu_y = 0.063 \text{ Hz}$. The frequency resolution is $7.7 \cdot 10^{-5} \text{ Hz}$ and the duration of the run is 4.3 d. Bottom plot: GGG has been set in rotation at $\nu_{spin} = 0.19 \text{ Hz}$, the natural oscillation frequency (resonance) during rotation is $\nu_w = \sqrt{(\nu_x^2 + \nu_y^2)}/2 = 0.098 \text{ Hz}$ and the same force signal is applied, which is up-converted close to the spin frequency and therefore now acts above resonance. The experimental data –i.e. the relative displacements of the test cylinders as given by one of the rotating capacitance bridges which read this differential displacements of the test cylinders– have been demodulated back to the non rotating horizontal plane of the lab for comparison with non rotating case shown above along the X direction. If GGG were an oscillator in 1-D only, a force signal applied above resonance would have been attenuated in this case by a factor 2.56; instead, the experimental data show no such attenuation. The frequency resolution is $1.16 \cdot 10^{-5} \text{ Hz}$ and the duration of the run is 19 d. We note in passing that in the non rotating case (top plot) noise increases at lower frequencies as expected for electronics noise, while in the rotating case the relevant electronics noise is that at the rotation frequency.

3 GGG sensitivity as compared to target in space

GGG is the lab prototype of the GG experiment in space and in this respect its task is to demonstrate that it can reach a sensitivity relevant to the GG target signal, namely the differential acceleration $\Delta a_{GG} \simeq 8 \cdot 10^{-17} \text{ m/s}^2$ (see Sec. 2, eq. (5)) which requires to detect – at the signal frequency $\nu_{orb} \simeq 1.7 \cdot 10^{-4} \text{ Hz}$ – relative displacements between the test masses

$$\Delta r_{GG} \simeq 0.5 \text{ pm} \quad (7)$$

with natural frequency $\omega_n = 2\pi/540 \text{ sec}^{-1}$. In order to establish the relevance of GGG to the GG space experiment we must take into account the following:

i) at 1-g the GGG test masses cannot be coupled as weakly as they can be coupled in absence of weight in space; since the sensitivity improves as the inverse of the natural coupling frequency squared, the ratio of the two is bound to be of about 3 orders of magnitude (at present is about 3000, it can be reduced by a factor 3). This means that GGG is bound to reach a limiting acceleration sensitivity (at ν_{orb}) about 3 orders of magnitude worse than the GG target (5);

ii) two noise sources which affect GGG are not present in the GG experiment in space: motor and bearings noise (GG does not require a motor to spin) and local terrain noise (the space experiment is performed in a lab –the GG spacecraft– which is isolated in space and co-rotating). GGG must reduce these noise sources below its limiting acceleration sensitivity, so that we can be confident that GG in space –thanks to its weaker coupling (i.e. lower natural frequency) and the absence of these noise sources– can reach (at the same frequency) its target acceleration sensitivity.

Fig. 5 shows that, at ν_{orb} the current SD in GGG displacement noise (obtained from raw data; see figure caption) is $\Delta r_{\nu_{orb}}/\sqrt{\text{Hz}} \simeq 3 \cdot 10^{-7} \text{ m}/\sqrt{\text{Hz}}$, which in a 30 d typical GGG run amounts to a displacement noise $\Delta r_{\nu_{orb}} \simeq 1.86 \cdot 10^{-10} \text{ m}$. The GGG rotating test masses in this run are coupled with a natural whirl frequency $\nu_w = 0.098 \text{ Hz}$, thus the SD in acceleration noise is $\Delta a_{\nu_{orb}}/\sqrt{\text{Hz}} \simeq 1.14 \cdot 10^{-7} \text{ m/s}^2/\sqrt{\text{Hz}}$, yielding an acceleration sensitivity $\Delta a_{\nu_{orb}} \simeq 7 \cdot 10^{-11} \text{ m/s}^2$, which is 6 orders of magnitude worse than the GG target (5). Since GGG at present has a coupling sensitivity a factor 2900 worse than GG, it is necessary to reduce the terrain and bearings noise sources by a factor 300. Then we will be sure that, once the test masses will be coupled as weakly as in GG in space where these noise sources are absent, the GG target acceleration sensitivity can be reached.

In order to reduce the current level of low frequency noise it is necessary to establish its physical origin. In the next Section we show experimentally that it is neither due to the electronics nor to local terrain noise (tilts and horizontal acceleration noise) and conclude that it is due to ball bearings noise affecting the shaft of the rotating system.

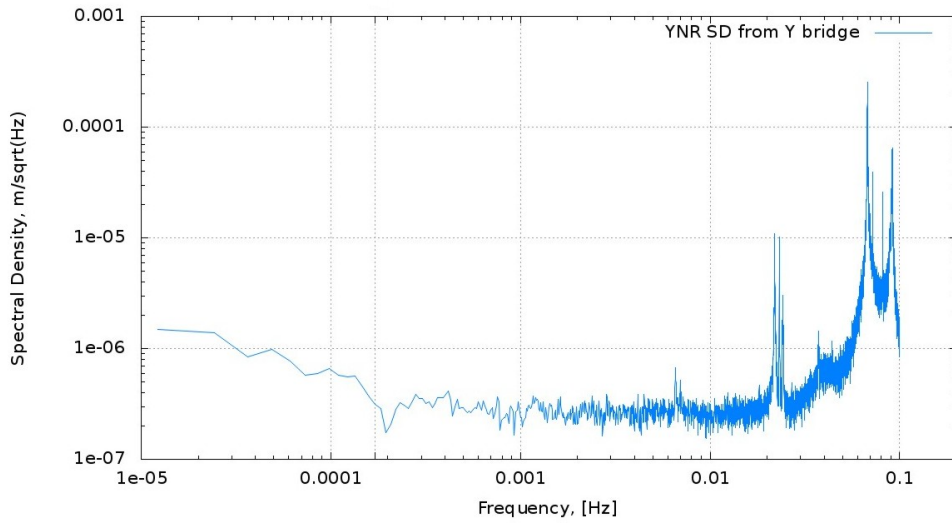


Figure 5: SD of the GGG displacement noise in one direction of the horizontal plane of the lab after demodulation from the rotating frame ($\nu_{spin} = 0.19$ Hz). The system is suspended from a 2-D non rotating laminar joint, no active tilt control is applied, thermal stability of the chamber is performed by electric heating. The plot is obtained from raw data. At the frequency $\nu_{orb} = 1.7 \cdot 10^{-4}$ Hz relevant for the GG experiment in space the SD in displacement noise is $3 \cdot 10^{-7}$ m/ $\sqrt{\text{Hz}}$. The natural coupling frequency of the rotating test masses is $\nu_w \simeq 0.098$ Hz

4 Assessment of low frequency noise sources

4.1 Read-out electronics noise

Differential displacements between the GGG test masses are measured in two perpendicular directions by two capacitance bridges co-rotating with the test masses. When the experiment rotates, the co-rotating bridge electronics noise contribution to the differential displacements low frequency noise is due to the co-rotating bridge electronics noise around the spin frequency. In order to establish this noise we have performed runs of the current (suspended) apparatus at zero spin. Fig. 6 shows the result of one such run performed with the Y capacitance bridge (two external signals were applied for other purposes). We can see that at 0.19 Hz, which is the value currently chosen to spin the system, the level of displacement noise is about $3 \cdot 10^{-8} \text{ m}/\sqrt{\text{Hz}}$, which is 1 order of magnitude lower than the (relevant) noise level reported in Sec. 3 at $1.7 \cdot 10^{-4} \text{ Hz}$ when the system spins.

When GGG rotates another source of low frequency noise can be due to slow variation of the bridge electronics gain. In presence of a constant displacement between the test masses in the not rotating frame the process of demodulation of the bridge signals modulated by the rotation translates slow variation of the bridge electronics gain into slow variations of the displacement, contributing to the low frequency noise. This effect was ruled out by checking the low frequency amplitude variations of a constant amplitude 10 mHz sinusoidal calibration force signal applied to GGG rotating as measured by the capacitance bridges.

We can then state that the present bridge electronics noise level is one order of magnitude lower with respect to the other sources of low frequency noise affecting the low frequency GGG measurements.

An improved read-out electronics is under completion which is estimated to provide 1 order of magnitude lower noise.

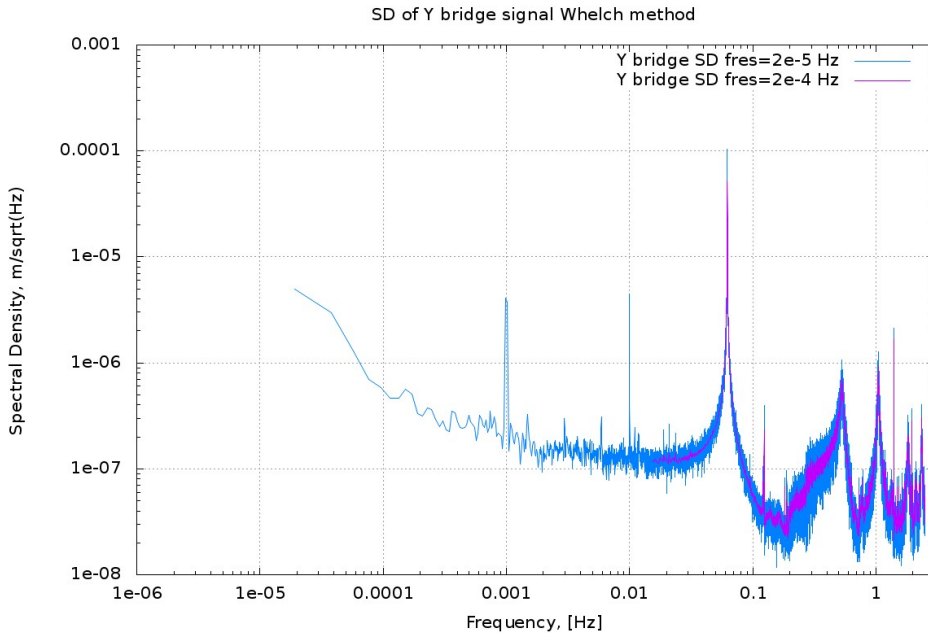


Figure 6: Spectral density of the relative displacements of the test cylinders along the Y direction when the system is not rotating (notice the natural differential frequency of the test cylinders along this direction at 0.07 Hz and the natural frequency of the suspended frame at 0.53 Hz). We can see that at 0.19 Hz, which is the frequency chosen for spin, the noise is about 1 order of magnitude smaller than reported in the run of Fig. 5. When the system spins at 0.19 Hz the electronics noise is the one reported here at this frequency, so we have about 1 order of magnitude room for improvement until we hit electronics noise. However, an improved read out electronics is under completion which is expected to perform 10 times better. Note that we have performed a run with a calibration signal applied of known fixed amplitude and we have checked that its amplitude does not have low frequency (in particular 1 d) variations. So, the gain of this electronics is not responsible for low frequency effects

4.2 Tilt and horizontal acceleration noise

The run reported in Fig. 1 (bottom plot) and Fig. 5 has been performed with the system weakly suspended from a 2-D non rotating laminar joint which provided a tilt attenuation at low frequencies by a factor 300 (as measured experimentally and reported elsewhere). This attenuation factor was 1 order of magnitude worse than expected and was attributed to the wires required to go through the joint from the frame rigid with the vacuum chamber to the weakly suspended frame.

After taking care of these wires, the tilt attenuation measured using two tiltmeters –one on the frame rigid with the chamber, one on the suspended frame– was a factor 5000, as reported in Fig. 7 (top plot).

We measured the tilt attenuation factor and the GGG sensitivity to tilts by applying a sinusoidal tilt and then by measuring the tilt on the suspended frame and at the same time the differential displacement between the GGG test masses. The experiment was not rotating. The frequency of the sinusoidal tilt signal applied to the upper plate was 10 mHz, its amplitude about 10 μ rad. The amplitude of the tilt measured on the suspended frame was about 2 nrad, see Fig. 7, top plot, giving the 5000 tilt attenuation factor.

In figure 8 (top plot) we report the measured differential displacement between the GGG test masses due to the applied tilt. It can be seen that the amplitude of the peak at 10 mHz is about 2 nm. From this measurement we conclude that to the 10 μ rad tilt applied to the upper plate corresponds a differential displacement of 2 nm, giving a GGG tilt sensitivity of about 0.2 nm/ μ rad.

It is interesting to study the measured tilt noise floor on the upper plate, see Fig. 7, bottom plot. This is a measurement of the tilt noise input to GGG. Because we don't know exactly the noise contribution due to the tiltmeter itself, we can conclude that the terrain tilt noise floor applied to sGGG is $\leq 10^{-6}$ rad/ $\sqrt{\text{Hz}}$. According to the measured GGG tilt sensitivity, to this measured input tilt noise should correspond a differential displacement of about $\leq 0.2 \cdot 10^{-9}$ m/ $\sqrt{\text{Hz}}$, that is a displacement noise three order of magnitude smaller with respect to the measured one. We can conclude that there are other sources of noise contributing to the measured GGG differential displacement signal noise.

The SD obtained from the two tiltmeters signals (Fig. 7, bottom plot) shows that the $\sim 10^{-7}$ rad/ $\sqrt{\text{Hz}}$ noise floor of the attenuated tilt signal is not reduced from the corresponding noise level of $\leq 10^{-6}$ rad/ $\sqrt{\text{Hz}}$ measured on the rigid frame by the same factor 5000. According to this tilt attenuation factor the ambient tilt noise transmitted to the suspended part of GGG should amount to some 10^{-10} rad/ $\sqrt{\text{Hz}}$. This is due to the noise level of the tiltmeters used (from Applied Geomechanics), such that the noise of the tiltmeter on the suspended frame is bigger with respect to the attenuated ambient tilt noise transmitted to the suspended frame by the thin suspension. The noise level of the Applied Geomechanics tiltmeters itself amounts then to the recorded $\sim 10^{-7}$ rad/ $\sqrt{\text{Hz}}$. The low frequency region of the same plot is dominated by the well known $1/f$ readout electronic noise and by the tiltmeters sensitivity to temperature variations.

It is now important to compare the estimated 10^{-10} rad/ $\sqrt{\text{Hz}}$ tilt noise floor on the suspended frame when the accelerometer inside it is not rotating (Fig. 7, bottom plot and the discussion above) with respect to the tilt noise measured when the accelerometer is rotating, shown in Fig. 8 bottom plot, though no tilt signal is applied at 0.01 Hz. It is apparent that tilt noise on the suspended frame with the accelerometer rotating inside it is four order of magnitude higher.

Since the shaft of the accelerometer rotates in ball bearings (a matched set of 4 bearings with ceramic balls) and the system frame + rotating accelerometer inside it is an isolated system, any bearings/shaft noise (very likely at low frequencies) will give rise to noise in the frame, that is recorded by the tiltmeter. Bearings noise was expected to manifest itself at some point, and it is most likely that it is now the limiting low frequency noise source which forbids the current level of tilt attenuation to be exploited.

A correlated issue was pointed out by JPL colleagues, namely the effect of horizontal acceleration noise, since we cannot perform a simple stringent test by applying a known horizontal acceleration signal (as we can do for a tilt signal). So, there was fear that horizontal accelerations would not be attenuated as effectively as tilts. It has been demonstrated theoretically that at the low frequencies of interest they are both attenuated by the same factor [9] and the result has also been checked with a numerical simulator developed in SymMechancis.

However, since ball bearings noise is the limitation when the accelerometer rotates, either we change from ball bearings to air bearings (as used in rotating torsion balances), which is a considerable experimental effort (see Sec. 6), or we move the 2-D weak joint on the shaft below the bearings, so that it can attenuate also the ball bearings noise (see Sec. 5. Such joint is now rotating, but it has been demonstrated also for GG that (for the same system) suspensions provide the same isolation level in the rotating and non rotating case (provided they do not loose their elastic properties, which is not the case here).

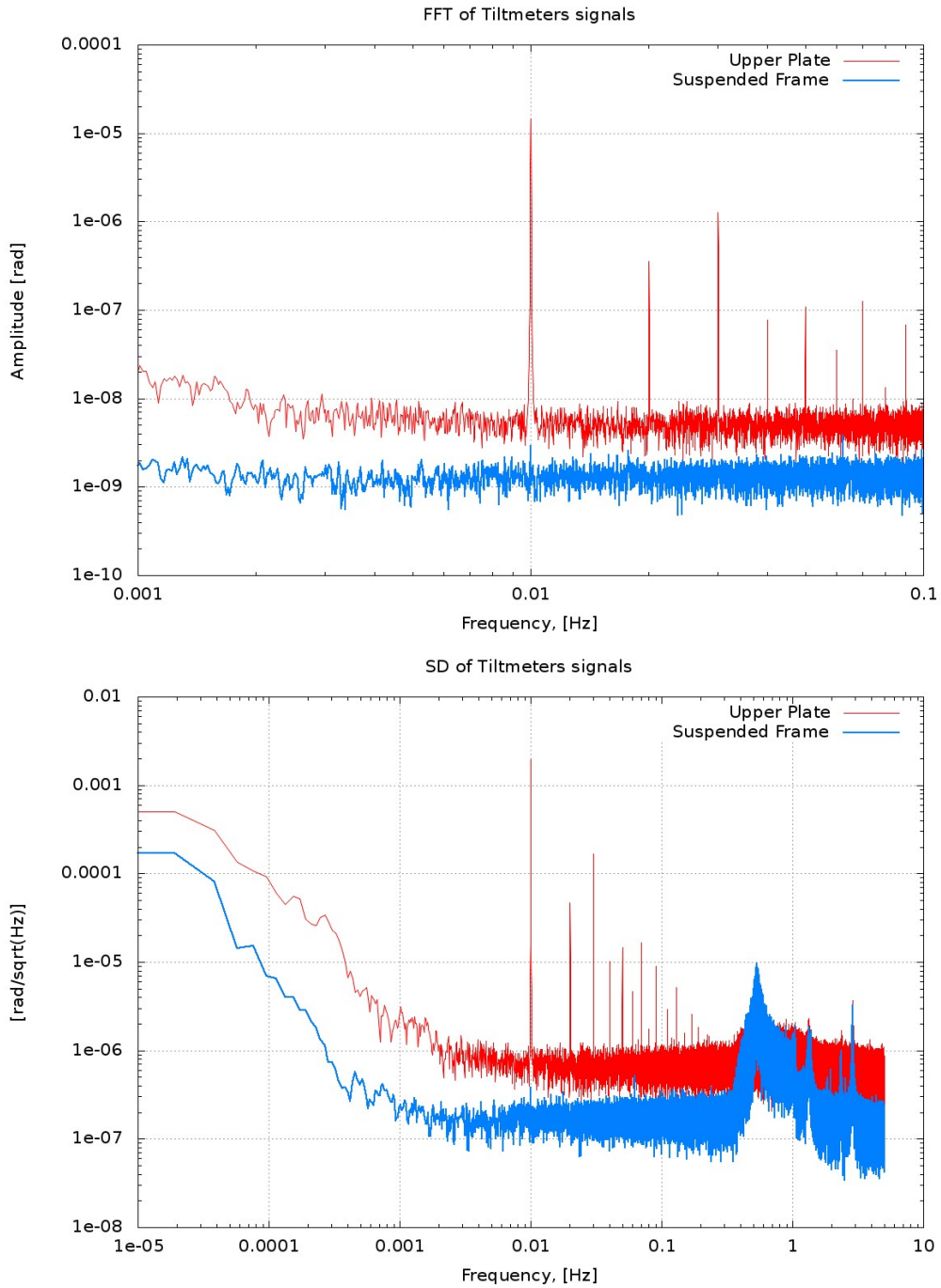


Figure 7: Top plot: FFT of data from one tiltmeter rigid with chamber (red) and another tiltmeter (blue) on the suspended non rotating frame housing the test masses (which in this test are not rotating). A tilt signal applied by means of PZTs on the top flange rigid with the chamber at 0.01 Hz is attenuated by a factor 5000. Bottom plot: Spectral density to show noise. The noise floor of the tiltmeter on the suspended frame (blue) is high because the tiltmeter has reached its sensitivity. Note also that tiltmeter measurements at very low frequencies are strongly affected by electronic $1/f$ noise and sensitivity to temperature variations.

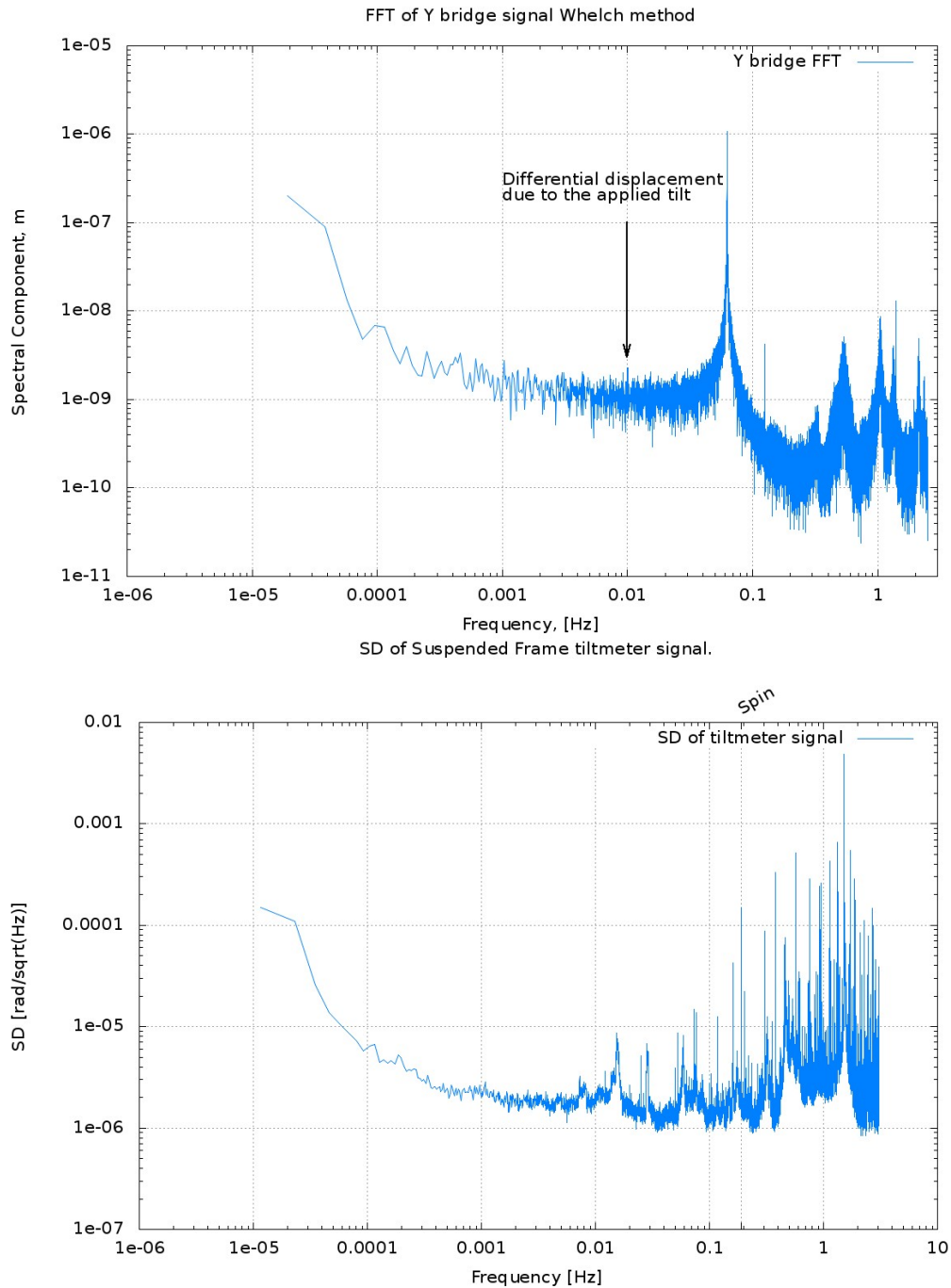


Figure 8: Top plot: FFT of the relative displacements of the test cylinders (while not rotating) recorded while the tilt signal was applied at 0.01 Hz. It is apparent that the attenuated tilt signal is just above the noise due to the readout electronics. Bottom plot: Spectral density of data recorded by the tiltmeter located on the suspended frame while the accelerometer inside it is rotating (no tilt signal is applied to the system). By comparison with Fig. 7, bottom plot we can see that now the noise recorded on the suspended frame is higher. Since suspended frame plus rotor is an isolated system, this must be due to the rotation of the rotor. We think that it comes from the ball bearings affecting the position of the rotor shaft.

4.3 Thermal stability

The level of thermal stability achieved inside the vacuum chamber housing the GGG experiment and the level of decoupling to 24 hr effects is reported in Fig. 9 and discussed in the caption.

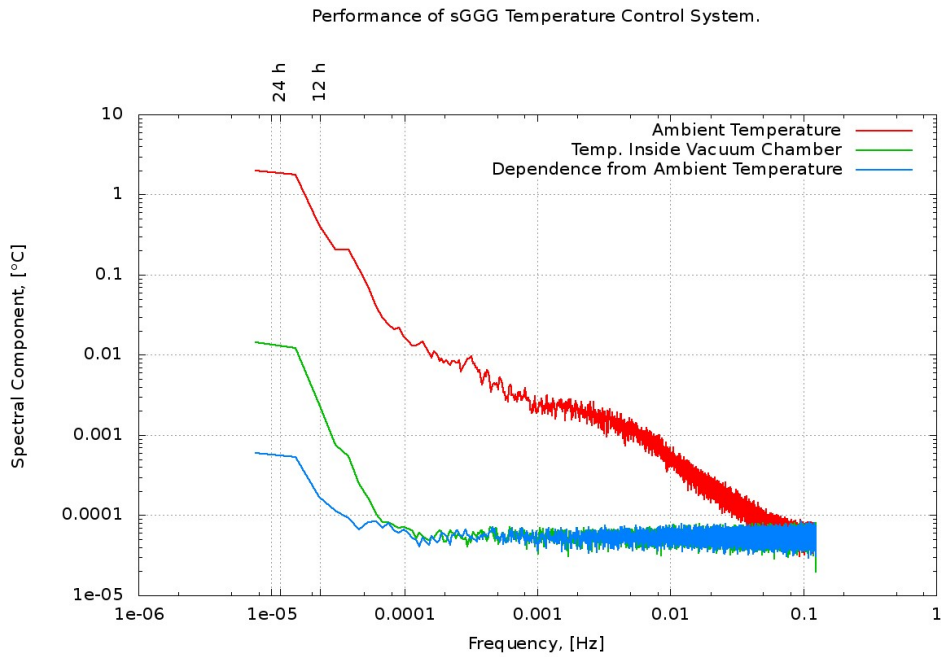


Figure 9: Performance of the Temperature Control System of the GGG experiment. 24h ambient temperature variations (red color plot) are attenuated inside the vacuum chamber (green color plot) by two order of magnitude. A precision 100 Ohm 10 ppm/°C resistor placed inside the vacuum chamber has been read out as one of the PT100 temperature sensors (blue color plot). 24h variations of these readings measure the dependence of the temperature control system with respect to the ambient temperature variations. At 24h period these variations are at the level of $7 \cdot 10^{-4} \text{°C}$ rms, giving an order of magnitude margin below the measured 24h temperature variations inside the chamber. We can then state that, within the reached level of 24h stabilization, the Temperature Control System is insensitive to ambient temperature variations.

5 Attenuation of ball bearings noise and expected improvements

In order to attenuate ball bearings noise along with terrain noise (tilts and horizontal accelerations) the current design of GGG could be modified as shown in Fig.10 by introducing the 2-D flexible joint on the GGG shaft. The 2-D flexible joint (11r) will strongly attenuate tilt and horizontal displacement noise introduced by the ball bearings (10) on the upper part of the shaft (9r). The solution for an eddy current damper in the rotating case (see Sec.6) can be implemented but may not even be needed because the amount of damping required is small. Overall the changes required are limited.

It is worth stressing that, in addition, in this improved design the rotor is no longer connected to the non rotating suspended frame as in the current situation, and this will reduce the effect of disturbances at low frequencies in the non rotating frame (mechanical coupling to the non rotating frame is no longer there).

Once ball bearings noise is reduced, terrain noise attenuation can be fully exploited and electronics noise from the capacitance read out will not be a limitation up to 2 orders of magnitude so as to come close to fill the sensitivity gap.

Then, the thickness of the lamellae of the test masses suspensions can be reduced so as to improve the coupling sensitivity of the proof masses by a factor four. This requires the terrain and bearing noise to be reduced accordingly. The implementation of air bearings presented in the next Section, which requires a considerable effort, will depend on these results.

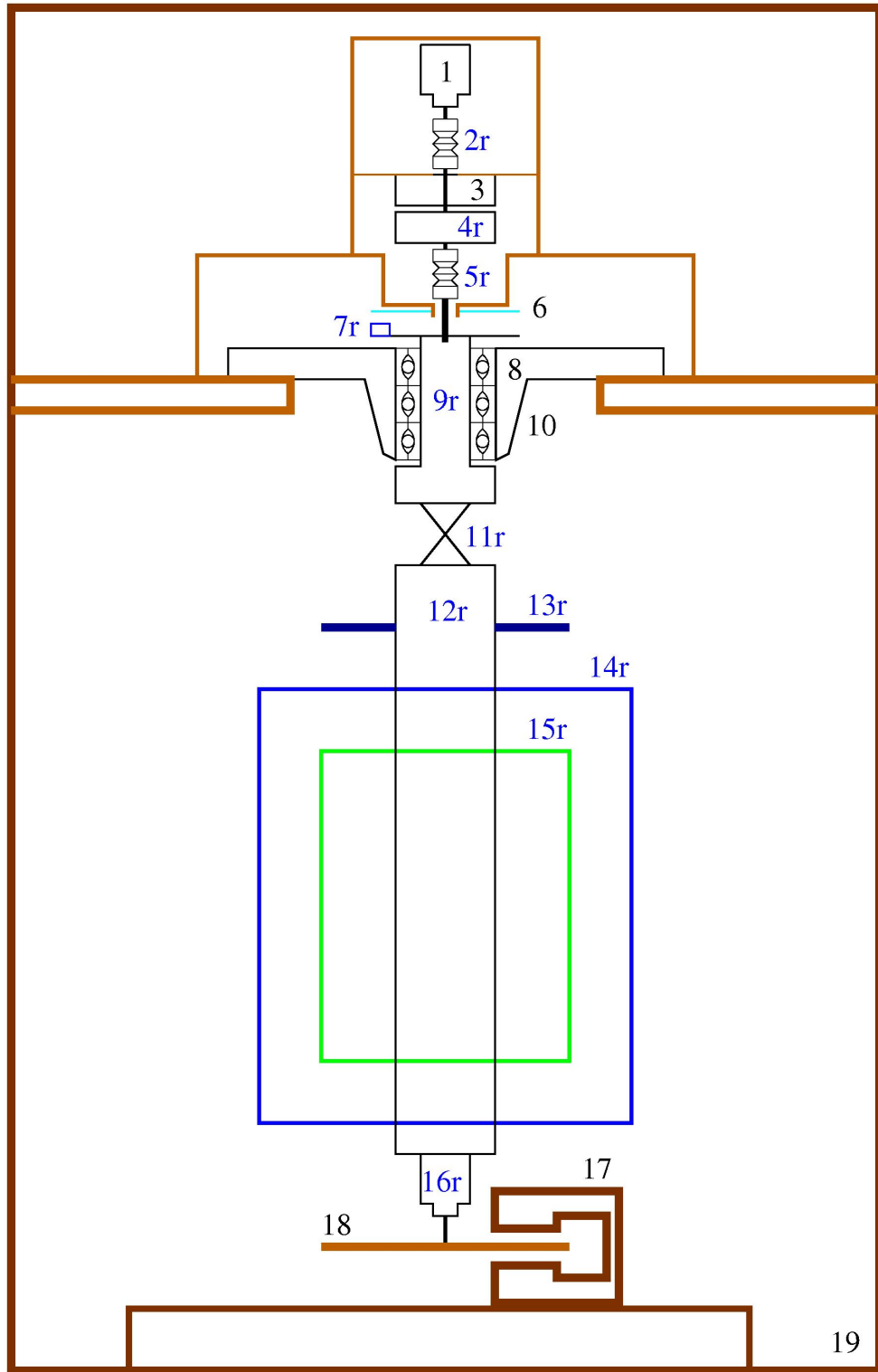


Figure 10: Attenuation of ball bearing noise by implementing a 2-D flexible joint on the shaft; The “r” suffix in the part numbering refers to rotating parts. 1: Main stepper motor. 2r and 5r: flexible joints. 3: rotating transformer primary coil, non rotating. 4r: rotating transformer secondary coil, rotating. 6: rotary encoder glass disk, not rotating. 7r: rotary encoder transducer, rotating. 8: plate holding the ball bearings, not rotating and fixed to the vacuum chamber. 9r: GGG shaft, rotating on ball bearing. 10: set of three ball bearings. 11r: 2-D flexible joint. 12r: suspended GGG shaft. 13r: rotating electronics board. 14r: outer test mass. 15r: inner test mass. 16r: eddy current damper stepper motor, fixed to the suspended part of the shaft (12r). 17: eddy current damper magnets, fixed to the bottom plate of the vacuum chamber (10). 18: eddy current damper plate, not rotating, fixed to the stepper motor (16r) shaft. 19: vacuum chamber

6 GGG design with air bearings and optical read-out

The implementation of an Air Bearing on GGG has been discussed during the meeting held at JPL on the week August 8–14, 2011.

We refer to Fig. 11, reporting the relevant components of the proposed implementation.

The air bearing (8r and 9) is intended to allow for the quiet rotation of the shaft (10r) while providing for lateral (due to its cylindrical part) and vertical (due to its planar part) stiffness against forces acting on it. The air bearing requires a small but continuous compressed air flow, so that it has been placed outside the vacuum chamber.

The GGG sensitive balance, composed of the two rotating hollow cylindrical test bodies (15r and 16r) differentially coupled in the horizontal plane, is suspended to the 2-D flexible joint (12r) with the purpose to insulate this part with respect to terrain tilts and horizontal accelerations. The 2-D flexible joint (12r) connects the suspended part of the shaft (13r) to the air bearing rotating part (8r).

The ferrofluid vacuum feedthrough (11) allows for the rotational motion transfer to the vacuum inside the chamber. It will be an Hollow Shaft Feedthrough housing the not-suspended part of the GGG shaft (10r). Stiffness against horizontal forces on the shaft (10r) due to the magnets needed by the vacuum feedthrough is provided by the cylindrical part of the air bearing, so that the ball bearing normally used on this type of feedthrough are avoided in this application.

The GGG shaft will then be rotating on the air bearing only. Free pendular oscillations of the 2-D flexible joint (12r) GGG suspended components are damped by an eddy current damper composed of a metallic plate (19) connected to the bottom end of the shaft (13r) and of a magnet (18) fixed to the bottom plate of the vacuum chamber. The eddy current damper, while damping the pendular motion of the rotating suspended shaft (13r), should not provide to it any DC horizontal force or coupling to its rotation. To this purpose the damper plate (19) should be not rotating. The stepper motor (17r) fixed to the rotating shaft (13r) will hold the damper plate on its shaft and will be driven in such a way to keep it not rotating. This rotating stepper motor will then be powered by the rotating transformer (3 and 4r) and driven by the rotating electronics board (14r) according to the rotation angle measured by the rotary encoder (6 and 7r) sending its readings to the rotating electronics board (14r).

In this advanced system an optical read out would be used, suggested by JPL, though not the based on the JPL laser gauge proposed for the space experiment (a report on this will be presented at a later time)

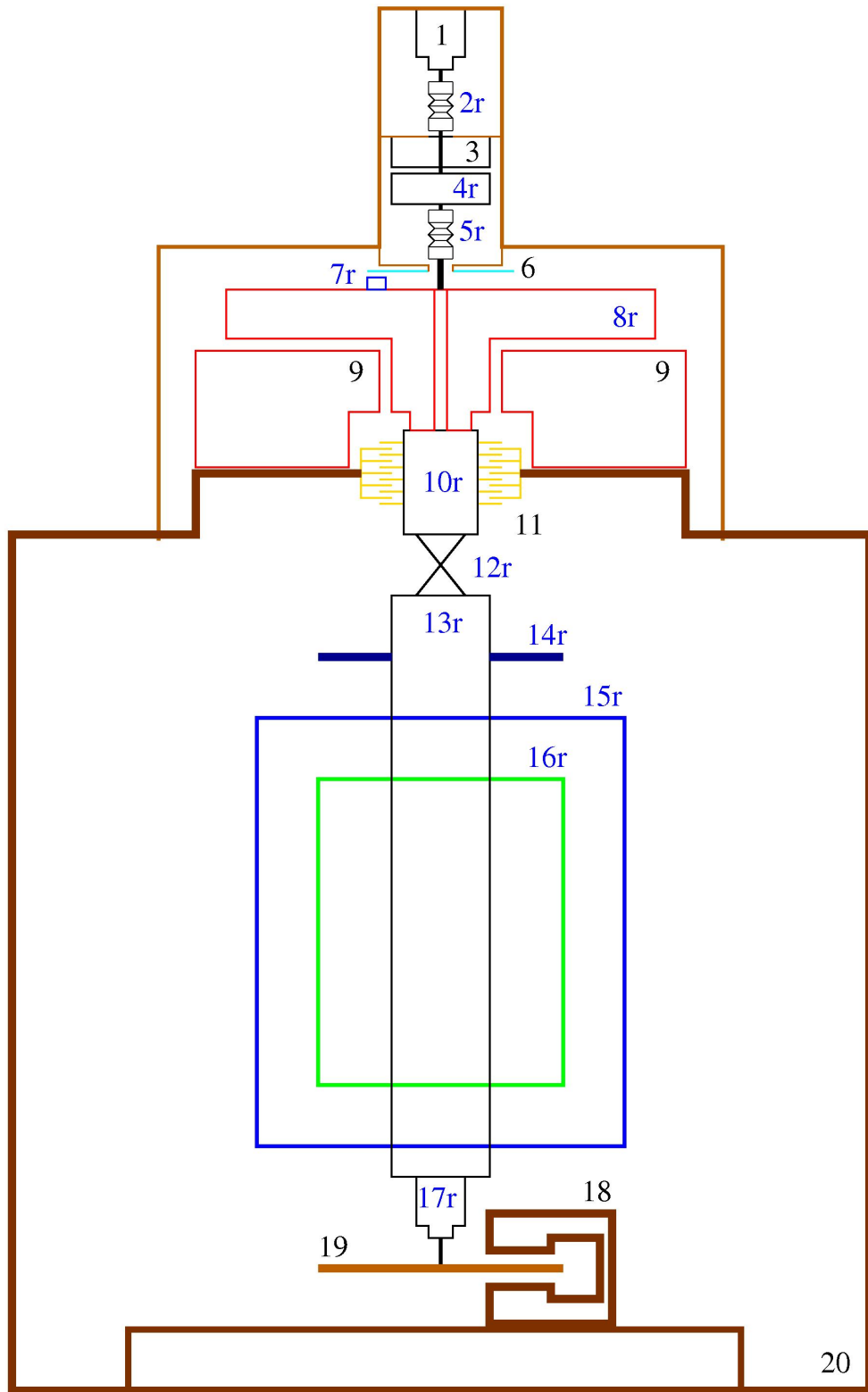


Figure 11: Main components of the proposed implementation of the air bearing solution for GGG; The “r” suffix in the part numbering refers to rotating parts. 1: Main stepper motor. 2r and 5r: flexible joints. 3: rotating transformer primary coil, non rotating. 4r: rotating transformer secondary coil, rotating. 6: rotary encoder glass disk, not rotating. 7r: rotary encoder transducer, rotating. 8r: air bearing, rotating part. 9: air bearing not rotating part. 10r: GGG shaft, rotating on air bearing. 11: ferro fluid feedthrough. 12r: 2-D flexible joint. 13r: suspended GGG shaft. 14r: rotating electronics board. 15r: outer test mass. 16r: inner test mass. 17r: eddy current damper stepper motor, fixed to the suspended part of the shaft (13r). 18: eddy current damper magnets, fixed to the bottom plate of the vacuum chamber (20). 19: eddy current damper plate, not rotating, fixed to the stepper motor (17r) shaft. 20: vacuum chamber.

References

- [1] S. Baekler et al., Phys. Rev. Lett. 83, 3585 (1999)
- [2] S. Schlamminger, Phys. Rev. Lett. 100, 041101 (2008)
- [3] S. Carusotto et al., Phys. Rev. Lett. 69, 1722–1725 (1992)
- [4] Fray et al., Phys. Rev. Lett. 93, 240404 (2004)
- [5] Pegna, Nobili, Shao et al., *Abatement of thermal noise in 2-D oscillators with rapidly rotating test masses*, Phys. Rev. D (decision from Phys. Rev. Lett. pending) (2011)
- [6] Pegna, Nobili, Shao et al., *Integration time in very high sensitive tests of the Equivalence Principle in space*, in preparation for PRD (2011)
- [7] Nobili, Shao, Pegna, Lucchesi et al., *Null checks in space experiments to test the Equivalence Principle*, in preparation for PRD (2011)
- [8] Pegna, Nobili, Shao et al., *Up-converting low frequency signals above resonance*, in preparation for Rev. Sci. Instr. (2011)
- [9] Pegna *Isolation of tilts and XY vibrations in sGGG*, Internal Note (2011)